ELSEVIER

International Journal of Heat and Fluid Flow 21 (2000) 499–505

International Journal of HEAT AND FLUID FLOW

www.elsevier.com/locate/ijhff

Turbulent budgets in rotating pipes by DNS

P. Orlandi *, D. Ebstein

Università di Roma "La Sapienza", Dipartimento di Meccanica e Aeronautica, via Eudossiana 18, 00184 Rome, Italy

Abstract

The budgets for the Reynolds stresses are given for a non-rotating and a rotating pipe at high rotation rates. The data have been obtained by fields generated by direct numerical simulations at $Re = 4900$. Particular emphasis has been placed on the near-wall region since background rotation modifies the wall structures. These budgets are useful to those interested in developing new one-point closure turbulence models for rotating flows.

1. Introduction

The study of turbulent flows through a pipe rotating about its axis is of interest for several flows in practical applications, for instance in combustors or rotating machineries. In addition, rotating flows occur in geophysical applications. The effects of solid body rotation on turbulence in a pipe presents similarities with three-dimensional boundary layers of practical importance, such as on swept wings of airplanes.

When a fluid enters a pipe rotating about its axis, tangential shear forces, acting between the wall and the fluid, cause the fluid to rotate with the pipe, resulting in a flow pattern different from that observed in a stationary pipe. Rotation reduces the turbulence in the wall region and increases it in the outer region due to the effects of centrifugal forces. Experimental results by Nishibori et al. (1987) and Reich and Beer (1989) indicate that the rotation changes the mean axial velocity profile, tending towards the parabolic profile characteristics of laminar flows. In addition, the creation of a mean azimuthal velocity, in the reference frame of the rotating pipe, does not make this flow unidirectional any longer. This component, negligible from the engineering point of view, allows one to investigate the performances of turbulence models. Hirai et al. (1988), for instance, showed that standard k–ϵ cannot generate this velocity component. From the physical point of view, however, a definite answer whether this component is Reynolds and rotation number independent still has not been reached.

Quite a large number of experimental studies have been dedicated to turbulent rotating pipes, up to values of $N = \Omega R/U_b = 5$. On the other hand, the numerical simulations are few, mainly due to the difficulties in treating the singularity at the axis. To avoid these difficulties, the simulations of rotating channel flow could be considered and this attempt was done by Oberlack et al. (1998). However, our opinion is that the rotating pipe, even if it necessitates of some attention on the numerics, avoids assumptions on the spanwise dimension of the rotating channel along its axis. In fact, in this case, the spanwise dimension should account for the formation of the large scale rolls at the center of the channel. The pipe has the further advantage of performing the comparisons with laboratory experiments. To our knowledge experiments on the rotating channel have not appeared in the literature, and, in our opinion, they should be very difficult to realize.

Orlandi and Fatica (1997) performed simulations for a rotating pipe for values of the rotation number N up to 2, and showed that the changes in turbulence statistics are due to the tilting of the near-wall streamwise vortical structures in the direction of rotation. The present study is an extension of the previous one. N has been increased up to 10, to examine numerically whether the phenomena observed experimentally by Nishibori et al. (1987) could be reproduced. They measured some of the Reynolds stresses at different values of N, but these profiles were mainly evaluated near the entrance of the pipe ($L_e/D < 100$) and not in the fully developed region. To our knowledge, no detailed experimental data on the Reynolds stresses are available yet for fully developed flows at high N. The other main objective of the present work lies in the evaluation of the Reynolds-stress budgets, a very easy task by the data from DNS. Even more important is to furnish the enstrophy budgets which are useful to obtain information on the effect of the rotation on the turbulent dissipation.

Although in simple flows, eddy viscosity models produce results comparable to those by Reynolds-stress models, the latter are necessary in a variety of flows that simpler models (k–ϵ) could not describe. The turbulent rotating pipe is one of them. Hirai et al. (1988) proved that the conventional k–ϵ model does not work for this flow. Even the Durbin (1991) model does not account for the rotation effects in the outer region of the pipe, whose effects could perhaps be modeled as suggested by Zeman (1995). We know that it is always more important to develop reliable Reynolds-averaged models for industries interested to design more efficient turbomachines. The Reynolds-stress equations contain several terms that must be modeled and that are difficult to measure. For instance, the

* Corresponding author. Tel.: +39-06-445-85878; fax: +39-06-484-854.

E-mail address: orlandi@navier.ing.uniroma1.it (P. Orlandi).

0142-727X/00/$ - see front matter
PII: S0142-727X(00)00037-0

pressure–strain correlation tensor, that for certain components is comparable to the production term, and to the rate of dissipation. Therefore, it is necessary to obtain these terms numerically.

The Reynolds number of the direct simulation is smaller than that occurring in practical applications where one-point closures are requested. LES were performed by Eggels et al. (1994) but these were limited at low N. Our point of view is that, to have reliable turbulence models for rotating pipes the near-wall region should be described. In the past, for the turbulent channel (Mansour et al., 1988) the DNS at low Reynolds numbers was of great help to the turbulence modelers (Durbin, 1991), thus, we think that, even more for this complex flow, the low Reynolds DNS should be of great help to model the wall region, and in particular at high rotation rates. To fully understand this complex flow a description of the modifications of the wall structures should be presented. We described these modifications in previous papers (Orlandi and Fatica, 1997; Orlandi, 1997) at $N = 2$; we observed, in this new set of simulations that there are no drastic changes when N increases. We are not showing again the results, but refer our previous papers.

2. Equations

The dimensionless Navier–Stokes equations in a reference frame rotating with the pipe wall are

$$\frac{D\mathbf{U}}{Dt} = -\nabla p + \frac{1}{Re}\nabla^2\mathbf{U} + N\mathbf{e}_z \times \mathbf{U}, \tag{1}$$

where it has been assumed that the rate of rotation Ω is direct along the axial direction z. The dimensionless equations have been obtained by taking the pipe radius R as reference length, the laminar Poiseuille velocity U_P, twice the bulk velocity U_b, as velocity scale. These quantities together with the kinematic viscosity ν give $Re = U_b D/\nu = U_P R/\nu$ and the rotation number $N = \Omega R/U_b$.

These equations can be solved when boundary conditions are assigned. This paper deals with the flow inside a circular pipe, hence no-slip conditions are assumed on the wall. As we are interested in the statistical steady state, periodicity is assumed along the streamwise direction, and this indicates that we are reproducing a fully developed rotating pipe. To prove, in addition, that the statistics represent a fully developed flow, it is important to advance the simulation for a sufficiently long time. In the present case, we performed the simulations starting from a coarse simulation; after a short transient the pressure gradient oscillates around a mean value. In this part of the simulations we have saved the fields that have been treated by a post-processing code to produce the statistics profiles. It has been also checked that the statistics do not change when a greater number of fields are used. The second order finite difference scheme in space and time developed by Verzicco and Orlandi (1996), briefly reported in Orlandi and Fatica (1997), has been used to solve Eq. (1). In the appendix of the latter paper the grid refinement checks were discussed. In that study the simulations were limited to $N = 2$; here the calculations have been extended to higher rotation rates $N = 5$ and $N = 10$. The results presented here are achieved by a $129 \times 96 \times 193$ grid. In a longer report by Ebstein (1998) it is shown that the results do not largely differ from those obtained by a coarse grid.

In simulations of rotating pipes an important parameter is the length of the pipe; it should be long enough to capture the stretching of the vortical structures due to the rotation rate as observed in the experiments by Nishibori et al. (1987). In all the simulations with $N > 0$ it was assumed $L_z/R = 25$, while for that at $N = 0$ L_z/R was set equal to 15. The only way to have a satisfactory answer about the issue whether the length of the pipe is sufficient or not, is by several simulations with different lengths and same resolution; hence this check should require a length $L_z/R = 50$ and 385 grid points in this direction. At this stage of the study we are interested to present the results in the reasonably long pipe rather than to spend a large computational time to check the independence of the correlations on L_z.

From the two-point correlations along z an idea about the flow structures is obtained. Thus the two-point correlations, at different distances from the wall, were evaluated and here only those at $y^+ = 20$ are presented. Fig. 1 shows that the correlations for v_r do not change by imposing the rotation; on the other hand the correlations for v_θ and v_z show that the structures are more elongated and that N affects the azimuthal more than the axial component. The correlation $R_{33} = \langle v_z' v_z' \rangle$ does not recover to zero indicating that the structures are spanning the full length of the pipe. Vorticity contour plots in Orlandi (1997) confirm this behavior and in addition show that the vortical structures are helicoidal.

Approximately 60 fields, separated by two time units, were saved and by a post-processing code the statistics and the budgets were evaluated. In all the quantities reported here, the overline accounts for time averages and $\langle\ \rangle$ for averages in the azimuthal and streamwise direction. In Fig. 2 the $\langle \overline{v_z} \rangle$ profiles in wall units indicate that, by increasing N, the log region disappears, hence turbulence models based on the law-of-the-wall should be discarded. The profiles of $\langle \overline{v_\theta} \rangle$ are not reported, these were given in Orlandi and Fatica (1997) and it

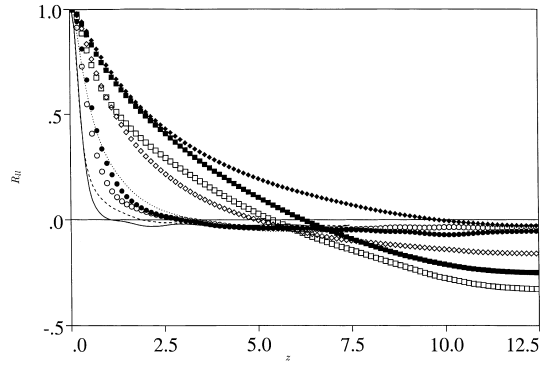

Fig. 1. Two-point velocity axial correlations (——, □ $R_{\theta\theta}$); (- - - -, ○ R_{rr}); (· · · · · ·, ◇ R_{zz}); lines $N = 0$, open symbols $N = 2$, closed symbols $N = 10$.

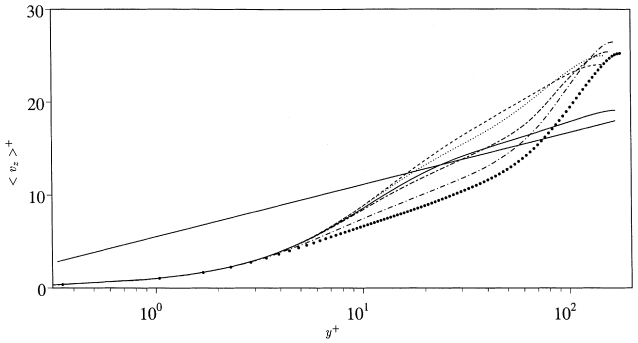

Fig. 2. Velocity profile in wall units (—— $N = 0$), (- - - - $N = 0.5$), (· · · · · · $N = 1$), (— - — $N = 2$), (— · — $N = 5$), (• $N = 10$).

was observed that the correction with respect to the solid body rotation decreases by increasing the rotation rate. In the experiments up to $N = 5$ by Reich and Beer (1989) $\langle \overline{v_\theta} \rangle$ was independent from N and Re. However, in more recent experiments by Imao et al. (1996) at $N = 0.5$ and $N = 1$ the data do not perfectly coincide with the theoretical parabolic profile and are slightly separated from each other. In our simulations it has been checked that at any N in the equation for $\langle \overline{v_\theta} \rangle$ and $\langle \overline{v_r} \rangle$, where the terms with $\langle \overline{v_\theta} \rangle$ appear, the balance is satisfied. From these arguments a definite answer on the independence of $\langle \overline{v_\theta} \rangle$ from N and Re cannot be drawn, more experiments and more refined simulations are necessary.

At low N the measurements by Imao et al. (1996) show that the normal stresses in the region far from the wall do not vary appreciably with the rotation, and this is confirmed by the simulations, even if in the DNS a substantial drop between $N = 0$ and $N = 0.5$ occurs near the wall. The condition is rather different at very high rotation rates. This is shown in Fig. 3 where the normal stresses profiles are not scaled by the friction velocity to emphasize the N dependence. At high values of N the normal stresses are affected in the whole pipe and in particular near the center. $\langle \overline{v'_\theta v'_\theta} \rangle^{0.5}$ increases everywhere, as well as $\langle \overline{v'_r v'_r} \rangle^{0.5}$, but near the wall less than near the center. $\langle \overline{v'_z v'_z} \rangle^{0.5}$ on the other hand decreases near the wall and increases at the center. We would like to point out that the profiles in a semilog scale emphasize the near-wall region. This choice is of particular utility when the DNS should guide the modeling of the wall region. As a general result, we observe that the rotation moves the peak of the turbulent kinetic energy away from the wall.

More drastic modifications occur for the turbulent stresses; in fact the rotation, breaking the symmetry, produces the stresses that are null in the non-rotating pipe. These stresses are given in Fig. 4(b) that shows a large $\langle \overline{v'_\theta v'_z} \rangle$ oscillating in r; these oscillations, almost absent at low rotation rates, are a consequence of the long spiral structures forming in the central region of the pipe. The figure in addition shows that the other two stresses have a much regular behavior, and that $\langle \overline{v'_\theta v'_r} \rangle$ is the smallest. Two of these stresses were measured by Imao et al. (1996) at low rotation rate and at $Re = 20000$, a value four times greater than the present ($Re = 4900$). Fig. 5 shows that, although there are differences between the numerical and experimental results, nevertheless the decrease of $\langle \overline{v'_\theta v'_z} \rangle$ with N and the points where it changes sign are reasonably well predicted. On the other hand, the differences for $\langle \overline{v'_z v'_r} \rangle$ should be attributed to the differences in Reynolds number. Orlandi and Fatica (1997) showed that the profile of the total stress follows the theoretical linear behavior and that the reduction of the pressure drop is not linear in N, different from that in Imao et al. (1996). The simulations at higher Reynolds number in principle could be done with the today's computers; this will be done, in the near future, to generate a new database at $N = 0.5$ and $N = 1$, since the fields for the low values of N were not saved. The database at the higher values of N has been used to evaluate the budgets, described in Section 3.

Before looking at the budgets for each component of the Reynolds stresses, we would like to point out that in this flow the Boussinesq hypothesis relating the turbulent stresses to the

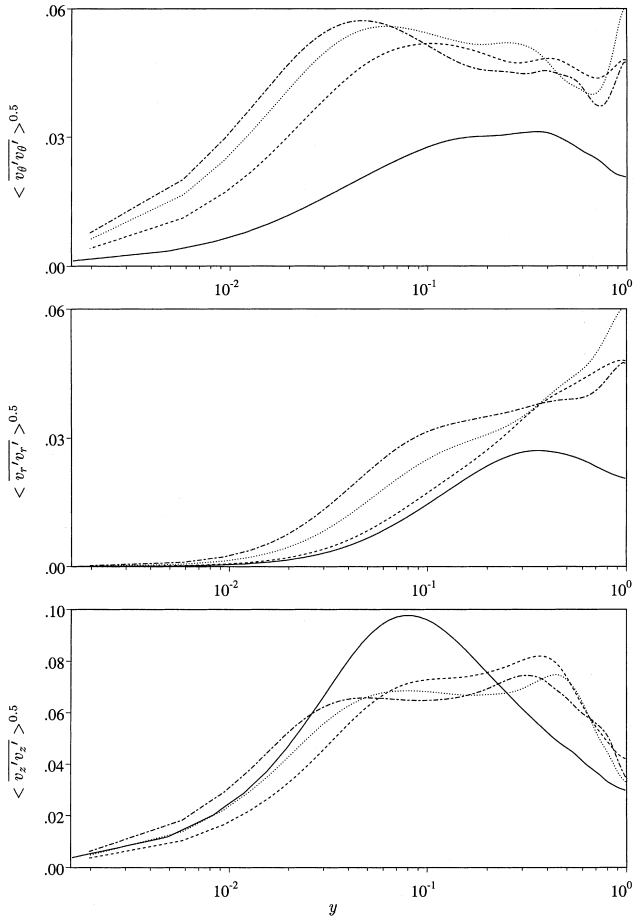

Fig. 3. Normal stress profiles (—— $N = 0$), (- - - - $N = 2$), (· · · · · · $N = 5$), (— - — $N = 10$).

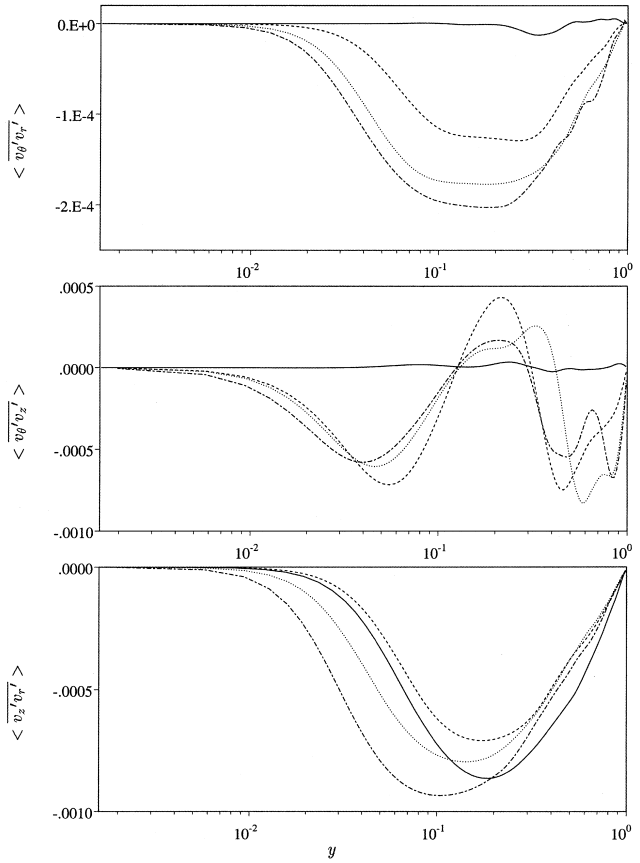

Fig. 4. Turbulent stress profiles (—— $N = 0$), (- - - - $N = 2$), (· · · · · · $N = 5$), (— - — $N = 10$).

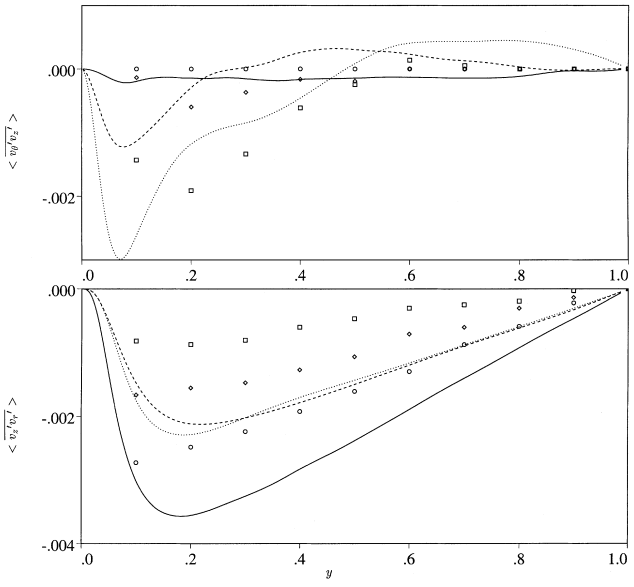

Fig. 5. Turbulent stress profiles compared with the Imao et al. (1996) data (——, ○ $N = 0$), (- - - - , □ $N = 0.5$), (· · · · · · , ◇ $N = 1$).

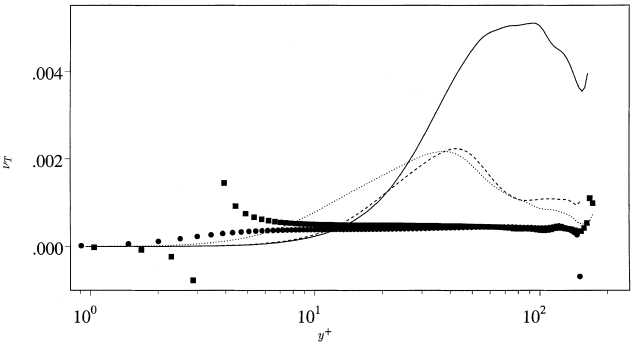

Fig. 6. Turbulent viscosity profiles (—— $N = 0$), (- - - - $N = 2$), (· · · · · · · $N = 10$) from $\langle \overline{v'_z v'_r} \rangle$, (• $N = 2$), (□ $N = 10$), from $\langle \overline{v'_\theta v'_r} \rangle$.

mean rate of strain, usually used in the k–ϵ closures cannot be used. In fact, $\langle \overline{v'_\theta v'_z} \rangle$ cannot be different from zero since $S_{\theta z} = 0$. The present database, in any case, permits one to see whether ν_T evaluated by dividing the $\langle \overline{v'_z v'_r} \rangle$ and $\langle \overline{v'_\theta v'_r} \rangle$ by the corresponding rate of main strain are consistent. Fig. 6 shows that the two eddy viscosities obtained by these turbulent stresses differ and in particular near the wall. This consideration confirms, once more, that for the rotating pipe it is mandatory to use the full Reynolds-stress turbulence models.

3. Budgets

Hirai et al. (1988) proved that the conventional k–ϵ model does not work and hence for rotating pipes the second order closure should be used. This statement suggests one to consider the equation of the Reynolds stresses, that at the steady state, and in the fully developed conditions are

$$\langle \overline{u_k} \rangle \frac{\partial R_{ij}}{\partial x_k} = -R_{ik} \frac{\partial \langle \overline{u_j} \rangle}{\partial x_k} - R_{jk} \frac{\partial \langle \overline{u_i} \rangle}{\partial x_k} + \nu \nabla^2 R_{ij} + \Pi_{ij} - \epsilon_{ij} - \frac{\partial S_{ijk}}{\partial x_k} - 2\left(e_{mki} \Omega_m R_{jk} + e_{mkj} \Omega_m R_{ik}\right). \quad (2)$$

The expression in cylindrical coordinates are not given; these are reported in the literature and can be found in Ebstein (1998). The Reynolds stresses are defined as $R_{ij} = \langle \overline{u'_i u'_j} \rangle$, in $S_{ijk} = \langle u'_i u'_j u'_k \rangle$ only the triple velocity correlations appear and

$$\Pi_{ij} = \left\langle \overline{u'_i \frac{\partial p'}{\partial x_j}} + \overline{u'_j \frac{\partial p'}{\partial x_i}} \right\rangle.$$

The rate of dissipation is

$$\epsilon_{ij} = 2\nu \left\langle \overline{\frac{\partial u'_i}{\partial x_k} \frac{\partial u'_j}{\partial x_k}} \right\rangle.$$

Equation (3.1), by inserting the Coriolis inside the convective term, can be written in the more simple form

$$0 = \mathrm{PD} + \mathrm{VD} + \mathrm{VP} + \mathrm{DS} + \mathrm{TD} + \mathrm{CT}, \quad (3)$$

where PD indicates production, VD the viscous diffusion, VP the correlation between velocity and pressure gradients, DS the rate of turbulent dissipation, TD the turbulent diffusion and CT indicates the convective term. Usually, the balance are normalized with respect to νu_τ^4; in dimensionless units this operation consists in dividing each term of Eq. (2) by $Re u_\tau^4$. To those interested in having the data in a different normalization, we would like to recall that $Re = 4900$ and that for N equal to 0, 2, 5, 10, u_τ respectively is 0.03475, 0.03214, 0.03405 and 0.0369. From these values it turns out that, different from what is expected, by increasing N up to $N = 2$ there is a drag reduction and then a drag increase. Nevertheless, the mean velocity profile tends to the laminar parabolic profile in the internal region of the pipe. This trend in the profiles perhaps is the reason why in the experiments it was extrapolated for the tendency to the relaminarization of the flow.

The budget for the turbulent kinetic energy at $N = 0$ agrees perfectly with the budget by Mansour et al. (1988) for the plane channel as it is shown in Fig. 7(a). In the turbulent kinetic energy equation the rate of solid body rotation does not appear directly, however, Fig. 7 shows the terms which are more affected by the rotation. Once more it is important to remember that simulations at low Re help to model the whole region of the pipe and in particular the near-wall region. Fig 7 shows that, indeed, in the near-wall region there is a large growth of the rate of dissipation (DS) and of the viscous diffusion (VD) balancing it. The turbulence production (PD) and the turbulent diffusion (TD) are less affected by N. The turbulent production for k coincides with the production term in the $\langle \overline{v'_z v'_z} \rangle$ equation, where N does not appear; hence the changes in (PD) are indirect. The production terms in the other two normal stresses cancel each other and their profiles show that the largest values occur in the log region, it contributes to the increase of these stresses with N (Fig. 3) near the centre. The analogue of Fig. 7 for each stress can be found in Ebstein (1998).

Fig. 7 shows a large change of the rate of dissipation, hence it is interesting to investigate whether the assumption $\epsilon_{ij} = \epsilon \delta_{ij}$, usually done in second order closures at high Reynolds numbers, is valid or not. In Fig. 8 the profiles of the ϵ_{ij}^+ for each N are given. About the possibility that $\epsilon_{ij} = \epsilon \delta_{ij}$ could be valid at high and not a low Re, from the data of the channel in Rodi and Mansour (1993), we observed that, indeed, by increasing by a factor of 2 the Reynolds number the profiles of ϵ_{ij}^+ do not change. Fig. 8 shows that the local isotropy assumption is not valid, and that, irrespective of N, ϵ_{rr} is always much smaller than the other two rates of dissipation. The rate of dissipation of the turbulent stresses are smaller than those of the normal stresses. By increasing N, in the wall region, $\epsilon_{\theta z}^+$ increases. It is interesting even to notice that only for $\langle \overline{v'_\theta v'_z} \rangle$ the near-wall region is important, for the other two ($\langle \overline{v'_z v'_r} \rangle$ and $\langle \overline{v'_\theta v'_r} \rangle$) in the

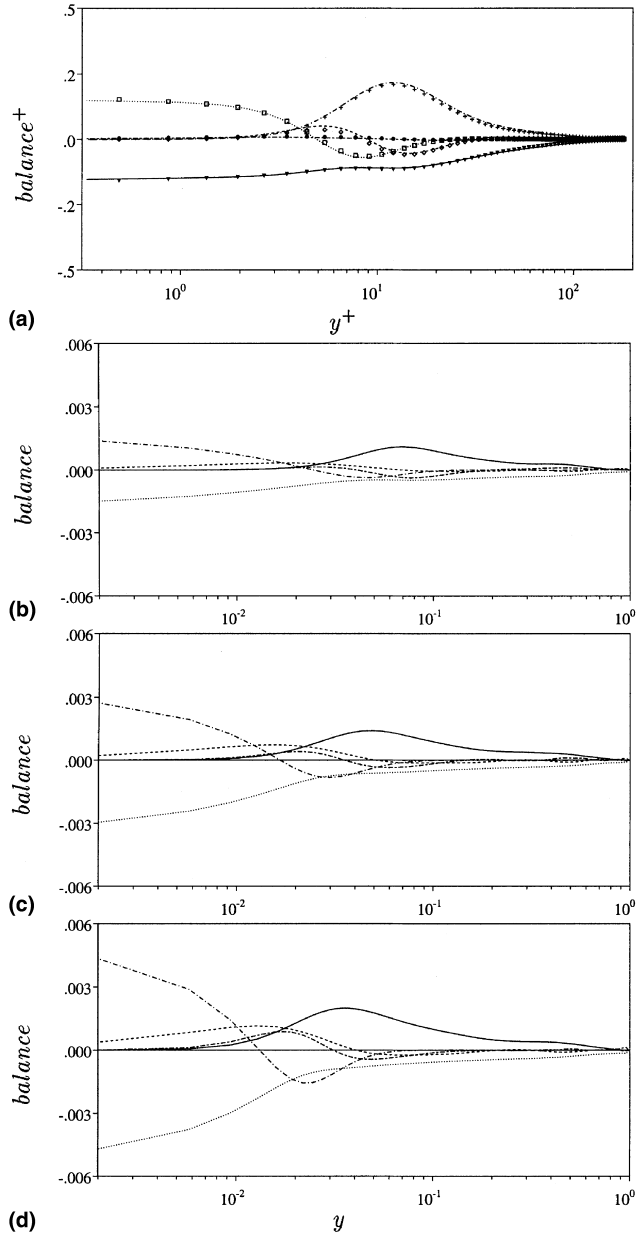

Fig. 7. Balance of the turbulent kinetic energy: (a) the symbols are from Mansour et al. (1988); the data are normalized with respect to vu_τ^4; (b) $N = 2$; (c) $N = 5$; (d) $N = 10$ in the dimensionless units of the simulations. (—— PD), (- - - - VP), (· · · · · · · DS), (— - — TD), (— · — VD).

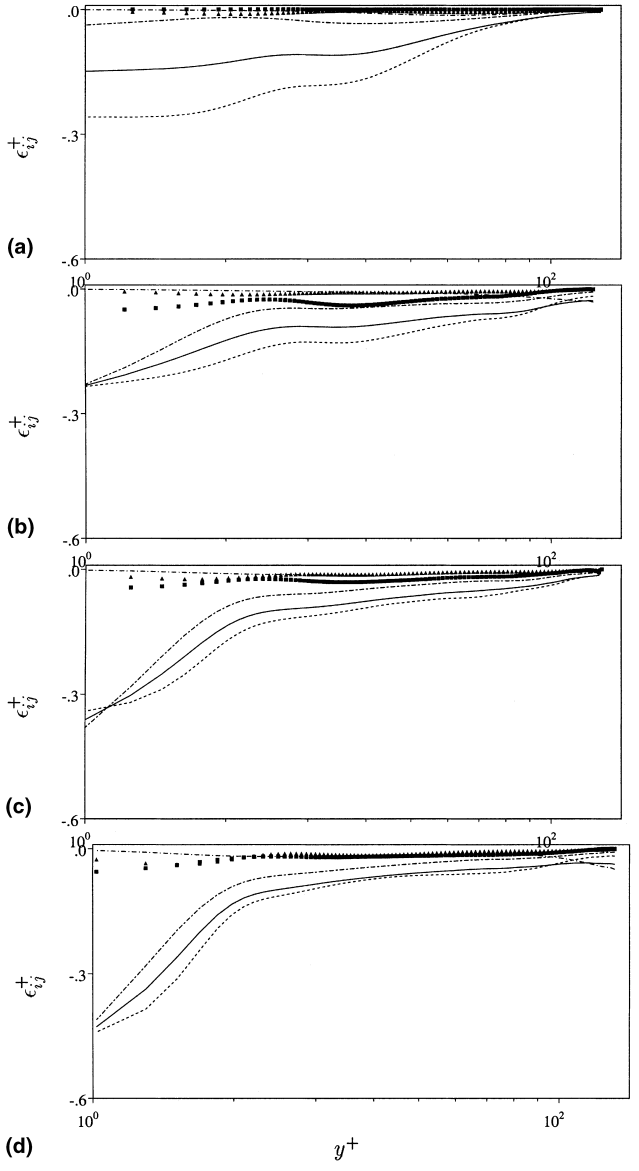

Fig. 8. Rate of dissipation profiles normalized with respect to vu_τ^4 as a function of y^+: (a) $N = 0$; (b) $N = 2$; (c) $N = 5$; (d) $N = 10$. (—— ϵ), (- - - - ϵ_{zz}), (— - — $\epsilon_{\theta\theta}$), (— · — ϵ_{rr}), (△ $\epsilon_{\theta r}$), (● ϵ_{zr}), (□ $\epsilon_{\theta z}$).

wall region the rate of dissipation is smaller than that near the center.

The balance for each turbulent stress shows that the terms largely dependent on N are VP and CT; N contributes directly to the latter. In Eq. (2), it has been observed that CT + VP is balanced by PR. As mentioned earlier, one of the major contributions of the DNS is to help to have new ideas on how to model the VP term; here we present for $N = 2$ the plots of this term split in the pressure–strain and in the pressure–transport terms together with CT. We would like to point out that at $N = 10$, VP and CT are of opposite sign and both are much greater than the other terms. The reason for this is related to the fact that the pressure in the simulation is the pressure in the rotating frame. Since VP + CT is comparable to the others, if each term is not appropriately modeled, it could produce wrong results. In Fig. 9, PS indicates the pressure–strain correlation, usually modeled explicitly in the second order closure, as for instance in Launder et al. (1975); PD is the pressure–transport term, usually included in the turbulent diffusion, which gives a zero contribution when integrated across the pipe. Fig. 9(a) shows that, near the wall, in the equation for $\langle\overline{v'_\theta v'_\theta}\rangle$, PS and PD balance and hence VP is negligible; in the outer region VP is close to CT and of opposite sign. CT prevails on VP giving a positive contribution to the production of $\langle\overline{v'_\theta v'_\theta}\rangle$; it explains why $\langle\overline{v'_\theta v'_\theta}\rangle$ increases with N in the central part of the pipe. Fig. 9(b) shows that for $\langle\overline{v'_r v'_r}\rangle$ CT has an opposite sign than for $\langle\overline{v'_\theta v'_\theta}\rangle$; it differs from PV and CT + PV contributes to increase $\langle\overline{v'_r v'_r}\rangle^{0.5}$ in the wall region as shown in Fig. 3(a).

The contributions of VP and CT, for the turbulent stresses, in Fig. 10(a) and (b) show that its magnitude is an order of magnitude greater than for the normal stresses. PS increases

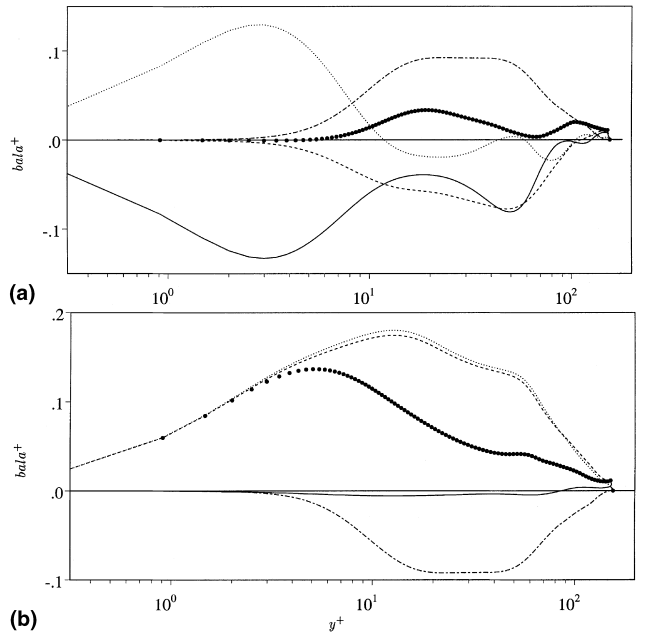

Fig. 9. Profiles of CT and VP terms and their combination, in wall units (νu_τ^4), for $N = 2$: (a) $\langle \overline{v'_\theta v'_\theta} \rangle$; (b) $\langle \overline{v'_r v'_r} \rangle$ as a function of y^+; (· · · · · · PD), (—— PS), (- - - - VP), (— — — CT), (• PV + CT).

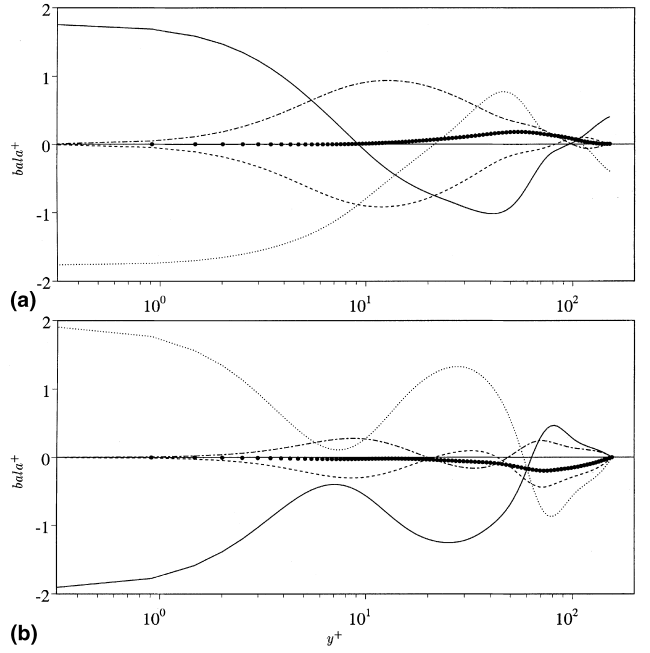

Fig. 10. Profiles of CT and VP terms and their combination, in wall units (νu_τ^4), for $N = 2$: (a) $\langle \overline{v'_\theta v'_r} \rangle$; (b) $\langle \overline{v'_z v'_r} \rangle$ as a function of y^+. Legend as in Fig. 9.

near the wall for effect of the rotation and, as for the non-rotating case, it is balanced by PD, this balance produces a small VP in the wall region, that at its turn is balanced by CT. Even if each term is large, the contributions of both are of the same order as that in the normal stresses in Fig. 9(a) and (b). In the central region of the pipe VP + CT for $\langle \overline{v'_\theta v'_r} \rangle$ counteracts the negative production; for $\langle \overline{v'_z v'_r} \rangle$ the behavior is similar, but there is an inversion of sign, since here VP + CT balances a positive production. This occurs also in the non-rotating case as it was shown by Mansour et al. (1988), we would like to point out that in the pipe some of the signs are opposite to those in the channel because in the pipe r is pointing towards the wall and in the channel y is pointing away from the wall.

If the budget of the Reynolds stresses is of large utility to get new ideas on near-wall one-point closures, of greater help is the enstrophy budget. DNS is the easy way to have such budgets and in particular to see how these are affected by the rotation rate. The enstrophy budget equation is

$$\left[U_j \frac{\partial \langle \overline{\omega_i^2} \rangle}{\partial x_j}\right] \frac{1}{2} = -\langle \overline{\omega_i \omega_j} \rangle S_{ij} - \langle \overline{\omega_i u_j} \rangle \frac{\partial \Omega_i}{\partial x_j} + \Omega_j \langle \overline{s_{ij} \omega_i} \rangle + \langle \overline{\omega_i \omega_j s_{ij}} \rangle - \nu \left\langle \overline{\left(\frac{\partial \omega_i}{\partial x_j}\right)^2} \right\rangle + \frac{\partial}{\partial x_j} \left[\nu \frac{\partial \langle \overline{\omega_i^2} \rangle}{\partial x_j} - \langle \overline{u_i \omega_i \omega_j} \rangle \right] \frac{1}{2}. \quad (4)$$

In this equation, the symbol indicating fluctuations has been omitted and the quantities averaged in time and in the homogeneous directions are indicated with capital letters. The terms on the right-hand side can be respectively indicated as

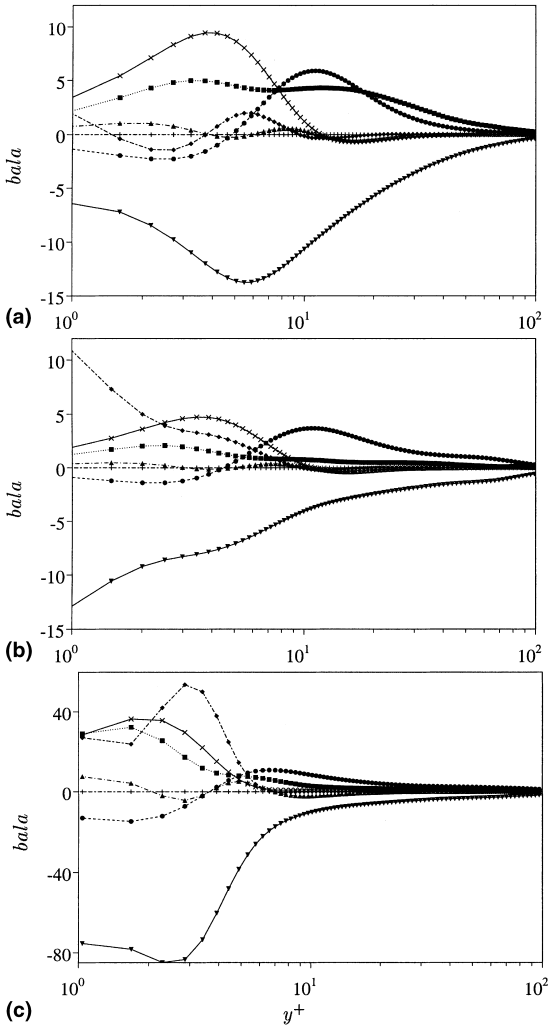

Fig. 11. Profiles of the enstrophy budget: (a) $N = 0$; (b) $N = 2$; (c) $N = 10$. ▽ DS, • PR, × CT, □ VP, △ TD, ◇ VD.

PR, PD, CT, VP, DS, VD, TD. The first impression, from the budgets at $N = 0,\ 2$ and $N = 10$ in Fig. 11(a)–(c), is that by increasing the rotation there are large variations in the near-wall region; in particular the magnitude of the rate of enstrophy dissipation increases with N. The profile of DS varies everywhere indicating large variations of the vorticity field. Orlandi and Fatica (1997) by contour plots of vorticity components showed that the vortical structures had a helical shape. Near the wall the enstrophy dissipation is balanced by the viscous diffusion and by CT and at $N = 10$ even VP becomes very important. At this point we do not want to discuss longer this balance even for the reason that, perhaps, minor changes can arise by more refined simulations. Fig. 11, however, permits one to get a first idea of the complex behavior of this balance and which are the more important terms.

4. Conclusions

The present study was performed in order to create a data base for turbulent rotating pipes at a low Reynolds number and at high N. At the moment a satisfactory number of fields are available for $N = 0,\ 2,\ 5$ and 10; for $N = 0.5$ and $N = 1$ some of the results were given by Orlandi and Fatica (1997). At that time the fields for these N were not saved and thus the balances were not calculated. The simulations do not take a long computational time and thus if there is a large demand of these budgets, we could perform the simulations again. Someone could argue that the present data are not validated as for example those for the turbulent channel by Kim et al. (1987); we are aware of this, but it should be taken into consideration that this flow has a more complex flow physics. In addition, the length of the pipe plays an important role and then a satisfactory streamwise resolution is difficult to achieve. We hope that in the near future other scholars will devote their time to perform DNS of this flow by a different numerical method, as for instance that developed by Loulou (1996).

A set of validated data for this flow are very important because the steady solution by one-point closure requires only the solution of a one-dimensional set of equations, hence the test of different closures is very fast. Despite the numerical simplicity the flow complexity remains and this requires satisfactory models. Only when good results for the rotating pipe are obtained will it be possible to achieve satisfactory results in practical applications such as swirling jets.

References

Durbin, P.A., 1991. Near-wall turbulence closure modeling without damping functions. Theoret. Comp. Fluid Dyn. 3, 1–13.

Ebstein, D., 1998. Reynolds stresses and kinetic energy budgets in the flow through an axially rotating pipe. Fourth year project of Aeronautical Engineering. Dept. of Aeronautics Imperial College, London.

Eggels, J.G.M., Boersma, B.J., Nieuwstadt, F.T.M., 1994. Direct and large eddy simulations of turbulent flow in an axially rotating pipe flow. Preprint.

Hirai, S., Takagi, T., Matsumoto, M., 1988. Prediction of the laminarization phenomena in an axially rotating pipe flow. J. Fluids Eng. 110, 424–430.

Imao, S., Itoh, M., Harada, T., 1996. Turbulent characteristics of the flow in axially rotating pipe. Int. J. Heat Fluid Flow 17, 444–451.

Launder, B.E., Reece, G.J., Rodi, W., 1975. Progress in the development of a Reynolds stress turbulence closure. J. Fluid Mech. 67, 537–566.

Loulou, P., 1996. Direct numerical simulation of incompressible pipe flow using a B-spline spectral method. Thesis. Department of Aeronautics and Astronautics, SUDAAR 683, Stanford University.

Mansour, N.N., Kim, J., Moin, P., 1988. Reynolds-stress and dissipation-rate budgets in a turbulent channel flow. J. Fluid Mech. 194, 15–44.

Nishibori, K., Kikuyama, K., Murakami, M., 1987. Laminarization of turbulent flow in the inlet region of an axially rotating pipe. JSME Int. J. 30, 255–262.

Oberlack, M., Cabot, W., Rogers, M.M., 1998. Group analysis, DNS and modeling of a turbulent channel flow with streamwise rotation. In: Proceedings of the 1998 Summer School, Stanford.

Orlandi, P., 1997. Helicity fluctuations in rotating and non-rotating pipes. Phys. Fluids A 9, 2045–2055.

Orlandi, P., Fatica, M., 1997. Direct simulations of a turbulent pipe rotating along the axis. J. Fluid Mech. 343, 43–72.

Reich, G., Beer, H., 1989. Fluid flow and heat transfer in axially rotating pipe 1. Effect of rotation on turbulent pipe flow. Int. J. Heat Mass Transfer 32, 551–561.

Rodi, W., Mansour, N., 1993. Low Reynolds number k–ϵ modeling with the aid of direct simulation data. J. Fluid Mech. 250, 509–529.

Verzicco, R., Orlandi, P., 1996. A finite difference scheme for direct simulation in cylindrical coordinates. J. Comp. Phys. 123, 402–414.

Zeman, O., 1995. The persistence of trailing vortices – a modeling study. Phys. Fluids 7, 135–143.